2

Stable Visual PID Control of Redundant Planar Parallel Robots

Miguel A. Trujano, Rubén Garrido and Alberto Soria
Departamento de Control Automático, CINVESTAV-IPN
México

This chapter presents an image-based Proportional Integral Derivative (PID) controller for a redundant overactuated planar parallel robot; the control objective is to drive the robot end effector to a desired constant reference position. The main feature of the proposed approach is the use of a vision system for obtaining the end effector position. This approach precludes the use of the robot forward kinematics. The Lyapunov method and the LaSalle invariance principle allow assessing asymptotic closed-loop stability. Experiments in a laboratory prototype permit evaluating the performance of the closed-loop system.

1. Introduction

Most of today industrial robots are controlled using joint-level PID controllers (Arimoto & Miyazaki, 1984; Wen & Murphy, 1990; Kelly, 1995; Spong, et al., 2005). In the case of parallel robots, their forward kinematics allows computing the end-effector position and orientation (Kock & Schumacher, 1998; Cheng et al., 2003); using the forward kinematics in real time may be computational demanding for some robot designs and sometimes it does not have an analytical solution; besides, a prior calibration procedure estimate the forward kinematics parameters. Any error in this estimation procedure would translate into positioning errors. An approach explored in this chapter is to use a vision system for measuring the end-effector coordinates; this methodology avoids solving in real time the forward kinematics and any calibration procedure. The chapter focuses on redundant planar parallel robots of the RRR-type studied in (Cheng et al., 2003) and shown in Fig. 1. This type of robot is well suited for laser and water cutting systems and in tasks requiring positioning in a plane. It is also worth remarking that over actuation reduces or even eliminates some kinds of singularities and improves Cartesian stiffness in the robot workspace.
Visual Servoing represents an attractive solution to position and motion control problems of autonomous robot manipulators evolving in unstructured environments (Corke, 1996; Hutchinson et al., 1996; Kelly, 1996; Papanikolopoulos & Khosla, 1993; Weiss et al., 1987; Wilson et al., 1996; Chaumette & Hutchinson, 2006 & 2007; Kragic & Christensen, 2005). There exist two approaches for this robot control strategy: camera-in-hand and fixed-camera. In the camera-in-hand configuration, the robot end-effector carries on the camera; the objective of this approach is to move the manipulator in such a way that the projection of a moving or static object is always at a desired location in the image given by the camera.

In contrast, in fixed-camera robotic systems, one or several cameras, fixed with respect to a global coordinate frame, capture images of the robot and its environment; the objective is to move the robot in such a way that its end-effector reaches a desired target. The proposed control law uses this later approach.

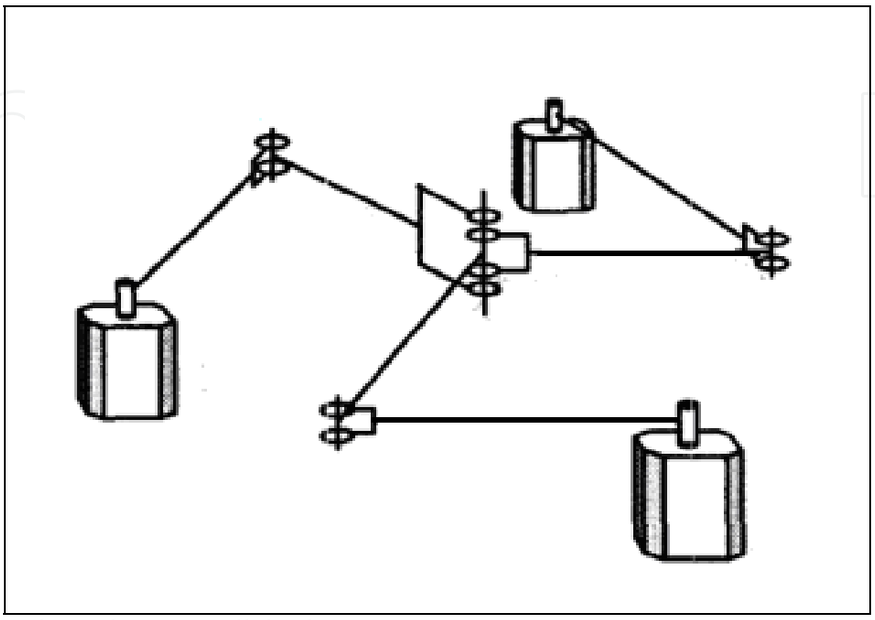

Fig. 1. Redundant planar parallel robot

Visual Servoing of parallel robots is an emerging field and until recently, some papers report interesting research in this area. Using a vision system in parallel robots allows calibrating their Forward Kinematics; moreover, in some instances it permits obtaining the position and orientation of some part of the robot mechanical structure thus dispensing the use of the Forward Kinematic for closed-loop control. Visual information of the robot legs allows controlling a Gough-Stewart parallel robot in (Andreff & Martinet, 2006) and (Andreff et al., 2007). Another interesting approach in (Dallej et al., 2007) shows how to control an I4R parallel robot using only visual feedback. Simulation results using a realistic robot model show satisfactory closed-loop performance. A visual control scheme, applied to the delta robot RoboTenis, is a key feature in (Angel et al., 2008) and (Sebastian et al., 2007). This approach uses the robot native joint controller as an inner loop, and a camera, which rests on the robot end-effector and closes an outer control loop; moreover, the authors show uniform ultimate boundedness of the tracking error. Experiments validate the proposed approach.

This Chapter proposes a control law that solves the position control problem for a redundant overactuated planar parallel robot by using direct vision feedback into the control loop; in this way, the proposed approach does not stem on solving the robot Forward Kinematics. The proposed algorithm exploits a PID-like control structure, similar to those proposed previously for open-loop kinematic chain robot manipulators (Kelly, 1998; Santibañez & Kelly, 1998). Moreover, compared with previous approaches on visual control of parallel robots, the stability analysis presented here, based on the Lyapunov method and the LaSalle principle, takes into account the robot dynamics. Experiments in a laboratory prototype permit assesing the performance of the closed-loop system.

2. Parallel robot modeling

A parallel manipulator is a closed-loop kinematic chain mechanism whose end-effector is linked to its base by several independent kinematic chains. References (Merlet, 2000; Tsai, 1999) describe a rather exhaustive enumeration of parallel robots mechanical architectures and their diverse applications are described in Singularities, which also appear in open chain robots, are abundant in parallel robots; when a manipulator is in a singular configuration, it loses stiffness and becomes uncontrollable. Singularities make the limited workspace of parallel manipulators even smaller. Redundant actuation is a method for removing singularities over the workspace; in this case, the number of actuators is greater than the number of end-effector coordinates. Besides removing singularities over the workspace, redundant actuation also has the advantages of making the robot structure lighter and faster, optimizing force distribution and improving Cartesian stiffness. The following paragraphs describe the modeling issues concerning the kinematics and dynamics of redundant planar parallel robots of the RRR-type.

2.1 Kinematics of parallel manipulators

The kinematic analysis of parallel robots comprises two parts: The Inverse Kinematics and the Forward Kinematics. In the Inverse Kinematics, given an end-effector position and orientation, the problem is to find the robot active joint values leading to these position and orientation. In the case of the Forward Kinematics, the robot active joint values are given and the problem is to find the position and orientation of the end-effector. As a rule, as the number of closed cinematic chains in the mechanism increases, the difficulty of the Forward Kinematics solution also increases, whereas the difficulty for the Inverse Kinematics solution diminishes.

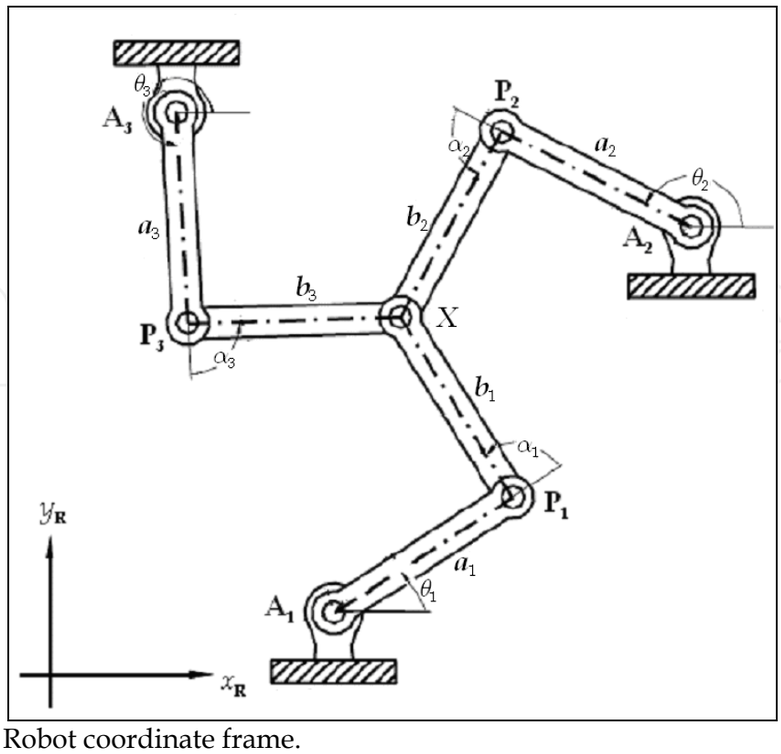

Fig. 2. Parallel Robot coordinate frame.

Figure 2 depicts a sketch of the redundant planar parallel robot. The robot kinematics assumes that all chain links have equal lengths, i.e. $L=a_i$ and $L=b_i$, $i=1,2,3$. Typically, a parallel robot has both active and passive joints; the robot actuators drive only the active joints. Symbol $\mathbf{A}_i$ represents the ith active joint with coordinates $\mathbf{X}_{\mathbf{A}_i}=\begin{bmatrix}x_{\mathbf{A}_i} & y_{\mathbf{A}_i}\end{bmatrix}^T$ with respect to the global Cartesian reference frame. Symbol $\mathbf{P}_i$ stands for the ith passive joint with coordinates $\mathbf{X}_{\mathbf{P}_i}=\begin{bmatrix}x_{\mathbf{P}_i} & y_{\mathbf{P}_i}\end{bmatrix}^T$. Variable $\mathbf{X}=\begin{bmatrix}x & y\end{bmatrix}^T$ defines the end-effector position, variable θ_i denotes the angle of the ith active joint, and variable α_i is the angle of the ith passive joint. These angles permits defining the active and passive joint position vectors

$$\mathbf{q_a}=\begin{bmatrix}\theta_1 & \theta_2 & \theta_3\end{bmatrix}^T, \tag{1}$$

$$\mathbf{q_p}=\begin{bmatrix}\alpha_1 & \alpha_2 & \alpha_3\end{bmatrix}^T. \tag{2}$$

Concatenating the above vectors produce a vector corresponding to all the robot joints

$$\mathbf{q}=\begin{bmatrix}\mathbf{q}_\mathbf{a}^T & \mathbf{q}_\mathbf{p}^T\end{bmatrix}^T. \tag{3}$$

Forward Kinematics

The following relationship describes the robot Forward Kinematics (Cheng et al., 2003)

$$x=\frac{\|\mathbf{X}_{\mathbf{P1}}\|^2(y_{\mathbf{P2}}-y_{\mathbf{P3}})+\|\mathbf{X}_{\mathbf{P2}}\|^2(y_{\mathbf{P3}}-y_{\mathbf{P1}})+\|\mathbf{X}_{\mathbf{P3}}\|^2(y_{\mathbf{P1}}-y_{\mathbf{P2}})}{2[x_{\mathbf{P1}}(y_{\mathbf{P2}}-y_{\mathbf{P3}})+x_{\mathbf{P2}}(y_{\mathbf{P3}}-y_{\mathbf{P1}})+x_{\mathbf{P3}}(y_{\mathbf{P1}}-y_{\mathbf{P2}})]}, \tag{4}$$

$$y=\frac{\|\mathbf{X}_{\mathbf{P1}}\|^2(x_{\mathbf{P3}}-x_{\mathbf{P2}})+\|\mathbf{X}_{\mathbf{P2}}\|^2(x_{\mathbf{P1}}-x_{\mathbf{P3}})+\|\mathbf{X}_{\mathbf{P3}}\|^2(x_{\mathbf{P2}}-x_{\mathbf{P1}})}{2[x_{\mathbf{P1}}(y_{\mathbf{P2}}-y_{\mathbf{P3}})+x_{\mathbf{P2}}(y_{\mathbf{P3}}-y_{\mathbf{P1}})+x_{\mathbf{P3}}(y_{\mathbf{P1}}-y_{\mathbf{P2}})]}, \tag{5}$$

$$\mathbf{X}_{\mathbf{P}i}=\mathbf{X}_{\mathbf{A}i}+L\begin{bmatrix}\cos\theta_i\\ \sin\theta_i\end{bmatrix},\ i=1,2,3. \tag{6}$$

It is worth remarking that the end-effector position $\mathbf{X}=\begin{bmatrix}x & y\end{bmatrix}^T$ does not depend on all the robot joint angles but only on the active joints angles θ_i. Therefore, it is possible to write down the robot Forward Kinematics as

$$\mathbf{X}=\varphi(\mathbf{q_a}). \tag{7}$$

Workspace

The set Ω defines the robot workspace; therefore, the end effector position must belong to this set, i.e. $\mathbf{X}\in\Omega\subset\mathbb{R}^2$. Fig. 3 shows workspace plots for $a_i=b_i=L$ and the general case $a_i\neq b_i$; variable d corresponds to the distance between the centers of two consecutive active joints. The robot under control has the configuration $a_i=b_i=L$, and $a_i+b_i<d$.

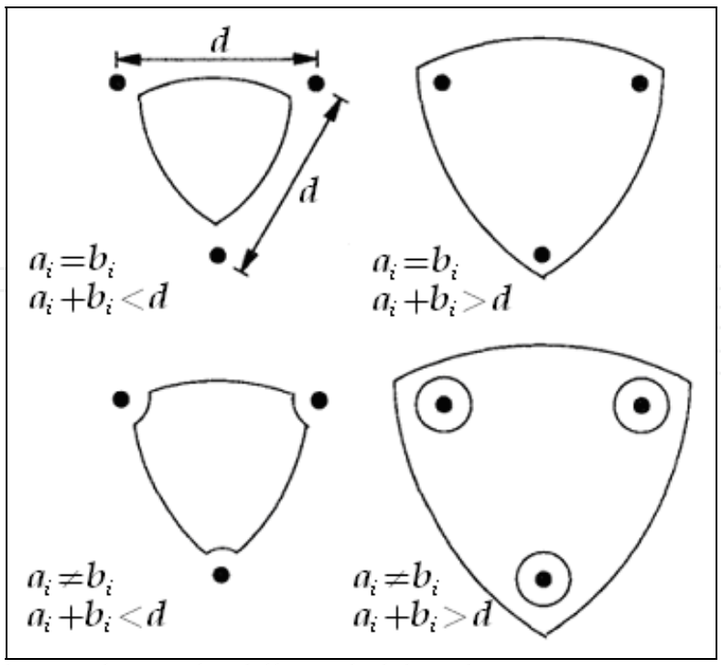

Fig. 3. Parallel Robot workspace for different link lengths.

Inverse kinematics

In this case the active joint angles depends only on the robot end-effector coordinates $\mathbf{X}$, i.e.

$$\theta_i = \arctan 2\left(\frac{\gamma_i}{\phi_i}\right) + \arctan 2\left(\frac{\pm\sqrt{\phi_i^2 + \gamma_i^2 - \xi_i^2}}{\xi_i}\right), \quad i = 1,2,3. \tag{8}$$

$$\begin{aligned} \phi_i &= 2L(x - x_{\mathbf{A}i}), \\ \gamma_i &= 2L(y - y_{\mathbf{A}i}), \\ \xi_i &= \|\mathbf{X} - \mathbf{X}_{\mathbf{A}i}\|^2. \end{aligned} \tag{9}$$

Subsequently, the active joint angles allows computing the passive joint angles as follows

$$\alpha_i = \operatorname{atan}\left(\frac{y - y_{\mathbf{A}_i} - l_1 \sin\theta_i}{x - x_{\mathbf{A}_i} - l_1 \cos\theta_i}\right) - \theta_i; \quad i = 1,2,3. \tag{10}$$

These solutions represent two different configurations for each leg that produce to $2^3 = 8$ solutions for the manipulator, as depicted in Fig. 4.

Configurations *a,* and *e* are preferable because they have shown more symmetric and isotropic force transmission throughout the workspace.

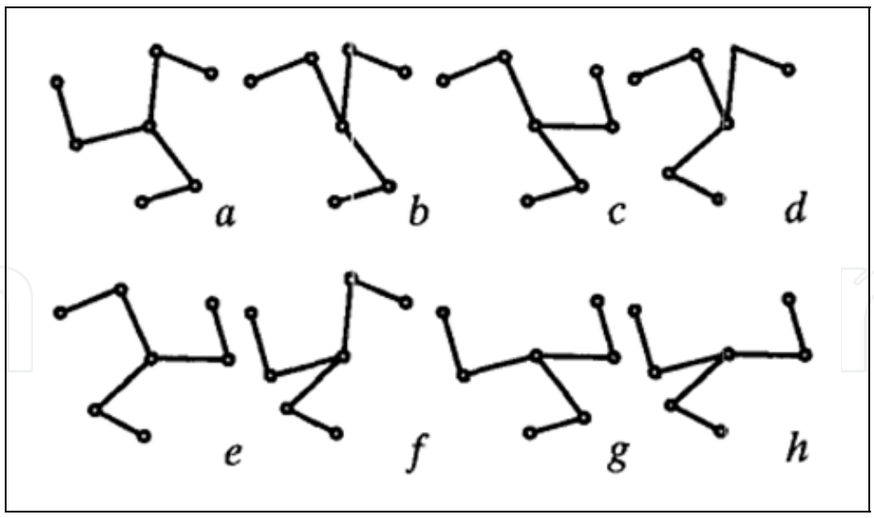

Fig. 4. All the solutions of the Parallel Robot inverse kinematics.

Differential kinematics

The following equations describe the relationship between the velocities at the joints and at the end effector

$$\dot{\mathbf{q}}_{\mathbf{a}} = \begin{bmatrix} \dot{\theta}_1 \\ \dot{\theta}_2 \\ \dot{\theta}_3 \end{bmatrix} = \begin{bmatrix} \frac{\cos(\theta_1+\alpha_1)}{L\sin\alpha_1} & \frac{\sin(\theta_1+\alpha_1)}{L\sin\alpha_1} \\ \frac{\cos(\theta_2+\alpha_2)}{L\sin\alpha_2} & \frac{\sin(\theta_2+\alpha_2)}{L\sin\alpha_2} \\ \frac{\cos(\theta_3+\alpha_3)}{L\sin\alpha_3} & \frac{\sin(\theta_3+\alpha_3)}{L\sin\alpha_3} \end{bmatrix} \begin{bmatrix} \dot{x} \\ \dot{y} \end{bmatrix} = \mathbf{S}\dot{\mathbf{X}}, \tag{11}$$

$$\dot{\mathbf{q}}_{\mathbf{p}} = \begin{bmatrix} \dot{\alpha}_1 \\ \dot{\alpha}_2 \\ \dot{\alpha}_3 \end{bmatrix} = \begin{bmatrix} -\frac{d_{1_x}}{L^2\sin\alpha_1} & -\frac{d_{1_y}}{L^2\sin\alpha_1} \\ -\frac{d_{2_x}}{L^2\sin\alpha_2} & -\frac{d_{2_y}}{L^2\sin\alpha_2} \\ -\frac{d_{3_x}}{L^2\sin\alpha_3} & -\frac{d_{3_y}}{L^2\sin\alpha_3} \end{bmatrix} \begin{bmatrix} \dot{x} \\ \dot{y} \end{bmatrix} = \mathbf{H}\dot{\mathbf{X}}. \tag{12}$$

$$\begin{aligned} d_{i_x} &= L\left[\cos\theta_i + \cos(\theta_i+\alpha_i)\right], \quad i=1,2,3. \\ d_{i_y} &= L\left[\sin\theta_i + \sin(\theta_i+\alpha_i)\right], \quad i=1,2,3. \end{aligned} \tag{13}$$

Concatenating (11) and (12) yields

$$\dot{\mathbf{q}} = \begin{bmatrix} \dot{\mathbf{q}}_{\mathbf{a}} \\ \dot{\mathbf{q}}_{\mathbf{p}} \end{bmatrix} = \begin{bmatrix} \mathbf{S} \\ \mathbf{H} \end{bmatrix} \dot{\mathbf{X}} = \mathbf{W}\dot{\mathbf{X}} \tag{14}$$

2.2 Dynamics of redundant planar parallel robot

In accordance with (Cheng et al., 2003), the Lagrange-D'Alembert formulation yields a simple scheme for computing the dynamics of redundantly actuated parallel manipulators; this approach uses the equivalent open-chain mechanism of the robot shown in Fig. 5. In

order to apply this scheme, the first step is to obtain a relationship between the joint torques associated to all the robot joints and the robot active joint torques. The following Proposition gives a method for obtaining this relationship

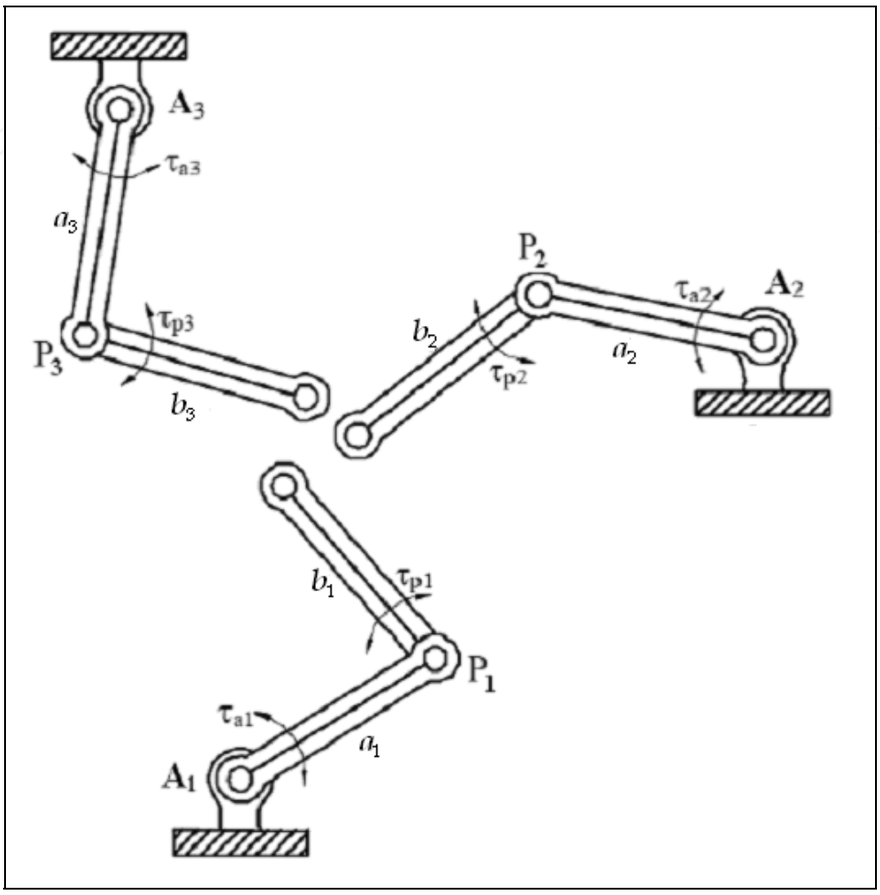

Fig. 5. Equivalent open-chain representation for the Parallel Robot.

***Proposition 1*:** Let the joint torque $\boldsymbol{\tau} \in \mathbb{R}^n$ of the equivalent open-chain system and the joint torque $\boldsymbol{\tau}_a$ of the redundantly actuated closed-chain system required to generate the same motion; then, both torques are related as follows

$$\mathbf{S}^T\boldsymbol{\tau}_a = \mathbf{W}^T\boldsymbol{\tau}. \tag{15}$$

***Proof of Proposition 1*:** We denote by $\mathbf{q}_e$ the vector of independent generalized coordinates of the mechanism. In the case of redundant actuation, the virtual displacement $\partial\mathbf{q}_a$ of the actuated joints is constrained. Using the kinematic constrains allows expressing $\mathbf{q}_a$ and $\mathbf{q}_p$ as

$$\mathbf{q}_a = \mathbf{q}_a(\mathbf{q}_e) \quad \text{and} \quad \mathbf{q}_p = \mathbf{q}_p(\mathbf{q}_e). \tag{16}$$

Differentiating the above equations gives

$$\delta \mathbf{q}_a = \frac{\partial \mathbf{q}_a}{\partial \mathbf{q}_e} \delta \mathbf{q}_e \quad \text{and} \quad \delta \mathbf{q}_p = \frac{\partial \mathbf{q}_p}{\partial \mathbf{q}_e} \delta \mathbf{q}_e. \tag{17}$$

Applying the above results to the Lagrange-D'Alembert equations yields

$$\begin{aligned} \left(\frac{d}{dt}\left(\frac{\partial L}{\partial \dot{\mathbf{q}}}\right) - \frac{\partial L}{\partial \mathbf{q}} - \boldsymbol{\tau}\right)^T \delta \mathbf{q} &= \left(\frac{d}{dt}\left(\frac{\partial L}{\partial \dot{\mathbf{q}}_a}\right) - \frac{\partial L}{\partial \mathbf{q}_a} - \boldsymbol{\tau}_a\right)^T \delta \mathbf{q}_a + \left(\frac{d}{dt}\left(\frac{\partial L}{\partial \dot{\mathbf{q}}_p}\right) - \frac{\partial L}{\partial \mathbf{q}_p} - \boldsymbol{\tau}_p\right)^T \delta \mathbf{q}_p \\ &= \left[\left(\frac{d}{dt}\left(\frac{\partial L}{\partial \dot{\mathbf{q}}_a}\right) - \frac{\partial L}{\partial \mathbf{q}_a} - \boldsymbol{\tau}_a\right)^T \frac{\partial \mathbf{q}_a}{\partial \mathbf{q}_e} + \left(\frac{d}{dt}\left(\frac{\partial L}{\partial \dot{\mathbf{q}}_p}\right) - \frac{\partial L}{\partial \mathbf{q}_p} - \boldsymbol{\tau}_p\right)^T \frac{\partial \mathbf{q}_p}{\partial \mathbf{q}_e}\right] \delta \mathbf{q}_e = 0. \end{aligned} \tag{18}$$

Variable $\boldsymbol{\tau}_p$ is the actuating torque on the passive joints. Since $\delta \mathbf{q}_e$ is now free to vary, the following expression follows from (18)

$$\left[\left(\frac{d}{dt}\left(\frac{\partial L}{\partial \dot{\mathbf{q}}_a}\right) - \frac{\partial L}{\partial \mathbf{q}_a}\right)^T, \left(\frac{d}{dt}\left(\frac{\partial L}{\partial \dot{\mathbf{q}}_p}\right) - \frac{\partial L}{\partial \mathbf{q}_p}\right)^T\right] \begin{bmatrix} \frac{\partial \mathbf{q}_a}{\partial \mathbf{q}_e} \\ \frac{\partial \mathbf{q}_p}{\partial \mathbf{q}_e} \end{bmatrix} - \left[\boldsymbol{\tau}_a{}^T \frac{\partial \mathbf{q}_a}{\partial \mathbf{q}_e} + \boldsymbol{\tau}_p{}^T \frac{\partial \mathbf{q}_p}{\partial \mathbf{q}_e}\right] = 0. \tag{19}$$

Or equivalently

$$\left[\frac{d}{dt}\left(\frac{\partial L}{\partial \dot{\mathbf{q}}}\right) - \frac{\partial L}{\partial \mathbf{q}}\right]^T \begin{bmatrix} \frac{\partial \mathbf{q}_a}{\partial \mathbf{q}_e} \\ \frac{\partial \mathbf{q}_p}{\partial \mathbf{q}_e} \end{bmatrix} = \boldsymbol{\tau}_a{}^T \frac{\partial \mathbf{q}_a}{\partial \mathbf{q}_e} + \boldsymbol{\tau}_p{}^T \frac{\partial \mathbf{q}_p}{\partial \mathbf{q}_e}. \tag{20}$$

Ignoring friction at the passive joints allows setting $\boldsymbol{\tau}_p = 0$. Note also that $\frac{d}{dt}\left(\frac{\partial L}{\partial \dot{\mathbf{q}}}\right) - \frac{\partial L}{\partial \mathbf{q}} = \boldsymbol{\tau}$.

These facts allow writing (20) as

$$\mathbf{W}^T \boldsymbol{\tau} = \mathbf{S}^T \boldsymbol{\tau}_a \tag{21}$$

$$\mathbf{W} = \begin{bmatrix} \frac{\partial \mathbf{q}_a}{\partial \mathbf{q}_e} \\ \frac{\partial \mathbf{q}_p}{\partial \mathbf{q}_e} \end{bmatrix} = \frac{\partial \mathbf{q}}{\partial \mathbf{q}_e} \tag{22}$$

$$\mathbf{S} = \frac{\partial \mathbf{q}_a}{\partial \mathbf{q}_e}. \tag{23}$$

The Euler-Lagrange's well-known formalism (Spong et al., 2005) allows modeling each of the legs of the open-chain mechanism in Fig. 5. Assuming that the robot moves in the horizontal plane, the following equations model the equivalent open chain mechanism

$$\bar{\mathbf{M}}_i\begin{bmatrix}\ddot{\theta}_i\\ \ddot{\alpha}_i\end{bmatrix}+\bar{\mathbf{C}}_i\begin{bmatrix}\dot{\theta}_i\\ \dot{\alpha}_i\end{bmatrix}+\bar{\mathbf{N}}_i=\begin{bmatrix}\tau_{\mathbf{a}_i}\\ \tau_{\mathbf{p}_i}\end{bmatrix},\ i=1,2,3 \tag{24}$$

where

$$\bar{\mathbf{M}}_i=\begin{bmatrix}\bar{M}_{i_{11}} & \bar{M}_{i_{12}}\\ \bar{M}_{i_{21}} & \bar{M}_{i_{22}}\end{bmatrix}=\begin{bmatrix}\lambda_i+2\beta_i\cos\alpha_i & \gamma_i+\beta_i\cos\alpha_i\\ \gamma_i+\beta_i\cos\alpha_i & \gamma_i\end{bmatrix},\qquad \bar{\mathbf{C}}_i=\begin{bmatrix}\bar{C}_{i_{11}} & \bar{C}_{i_{12}}\\ \bar{C}_{i_{21}} & \bar{C}_{i_{22}}\end{bmatrix}=\begin{bmatrix}-\beta_i\dot{\alpha}_i\sin\alpha_i & -\beta_i\left(\dot{\alpha}_i+\dot{\theta}_i\right)\sin\alpha_i\\ \beta_i\dot{\alpha}_i\sin\alpha_i & 0\end{bmatrix}$$

$$\lambda_i=m_{i1}{r_{i1}}^2+I_{i1}+m_{i2}\left(a_i^2+r_{i2}^2\right)+I_{i2},\ \beta_i=m_{i2}a_i r_{i2},\ \gamma_i=m_{i2}{r_{i2}}^2+I_{i2}$$

Parameters I_{ij}, m_{ij} and r_{ij}, $i,j:1,2,3$, correspond to the inertia, mass, and center of mass of each link. Combining the equations described above gives the dynamics of the open-chain system in the form

$$\bar{\mathbf{M}}\ddot{\mathbf{q}}+\bar{\mathbf{C}}\dot{\mathbf{q}}+\bar{\mathbf{N}}=\boldsymbol{\tau} \tag{25}$$

$$\bar{\mathbf{M}}=\begin{bmatrix}\bar{M}_{1_{11}} & 0 & 0 & \bar{M}_{1_{12}} & 0 & 0\\ 0 & \bar{M}_{2_{11}} & 0 & 0 & \bar{M}_{2_{12}} & 0\\ 0 & 0 & \bar{M}_{3_{11}} & 0 & 0 & \bar{M}_{3_{12}}\\ \bar{M}_{1_{12}} & 0 & 0 & \bar{M}_{1_{22}} & 0 & 0\\ 0 & \bar{M}_{2_{12}} & 0 & 0 & \bar{M}_{2_{22}} & 0\\ 0 & 0 & \bar{M}_{3_{12}} & 0 & 0 & \bar{M}_{3_{22}}\end{bmatrix},\quad \bar{\mathbf{C}}=\begin{bmatrix}\bar{C}_{1_{11}} & 0 & 0 & \bar{C}_{1_{12}} & 0 & 0\\ 0 & \bar{C}_{2_{11}} & 0 & 0 & \bar{C}_{2_{12}} & 0\\ 0 & 0 & \bar{C}_{3_{11}} & 0 & 0 & \bar{C}_{3_{12}}\\ \bar{C}_{1_{21}} & 0 & 0 & 0 & 0 & 0\\ 0 & \bar{C}_{2_{21}} & 0 & 0 & 0 & 0\\ 0 & 0 & \bar{C}_{3_{21}} & 0 & 0 & 0\end{bmatrix},\quad \bar{\mathbf{N}}=\begin{bmatrix}\bar{\mathbf{N}}_1\\ \bar{\mathbf{N}}_2\\ \bar{\mathbf{N}}_3\end{bmatrix},$$

$$\tau=\begin{bmatrix}\tau_{\mathbf{a}_1} & \tau_{\mathbf{p}_1} & \tau_{\mathbf{a}_2} & \tau_{\mathbf{p}_2} & \tau_{\mathbf{a}_3} & \tau_{\mathbf{p}_3}\end{bmatrix}^T$$

The term $\bar{\mathbf{M}}$ is the inertial matrix, $\bar{\mathbf{C}}$ the Coriolis and centrifugal force terms, and $\bar{\mathbf{N}}$ is a constant disturbance vector. The number of active and passive joints is n, $\mathbf{q_a}=\begin{bmatrix}\theta_1 & \theta_2 & \theta_3\end{bmatrix}^T\in\mathbb{R}^m$ stands for the active joints and $\mathbf{q_p}=\begin{bmatrix}\alpha_1 & \alpha_2 & \alpha_3\end{bmatrix}^T\in\mathbb{R}^{n-m}$ for the angles of the passive joints. In the same way, vectors $\boldsymbol{\tau}_\mathbf{a}=\begin{bmatrix}\tau_{\mathbf{a}_1} & \tau_{\mathbf{a}_2} & \tau_{\mathbf{a}_3}\end{bmatrix}^T\in\mathbb{R}^m$, $\boldsymbol{\tau}_\mathbf{p}=\begin{bmatrix}\tau_{\mathbf{p}_1} & \tau_{\mathbf{p}_2} & \tau_{\mathbf{p}_3}\end{bmatrix}^T\in\mathbb{R}^{n-m}$ correspond to the torques in the active and passive joints respectively. It is worth noting that in most parallel robots the angles of the active joints cannot play the role of generalized coordinates because their Forward Kinematics do not have a closed form solution., Therefore, it is not possible to write down the dynamic equations in terms of the active joints. For that reason, the development of the parallel robot dynamic model will consider the robot end-effector coordinates as a set of generalized coordinates, i.e. $\mathbf{q_e}=\mathbf{X}$. Substituting $\boldsymbol{\tau}$ in (25) into(21), we have

$$\mathbf{W}^T\left(\bar{\mathbf{M}}\ddot{\mathbf{q}}+\bar{\mathbf{C}}\dot{\mathbf{q}}+\bar{\mathbf{N}}\right)=\mathbf{S}^T\boldsymbol{\tau}_\mathbf{a}. \tag{26}$$

Taking the time derivative of (14) leads to

$$\ddot{\mathbf{q}}=\dot{\mathbf{W}}\dot{\mathbf{X}}+\mathbf{W}\ddot{\mathbf{X}} \tag{27}$$

Substituting $\dot{\mathbf{q}}$ and $\ddot{\mathbf{q}}$ given in(14) and (27) into (26) produces the following dynamic model

$$\mathbf{M}\ddot{\mathbf{X}}+\mathbf{C}\dot{\mathbf{X}}+\mathbf{N}=\mathbf{S}^T\boldsymbol{\tau}_\mathbf{a}, \tag{28}$$

where

$$\begin{aligned}\mathbf{M}&=\mathbf{W}^T\bar{\mathbf{M}}\mathbf{W},\\ \mathbf{C}&=\mathbf{W}^T\bar{\mathbf{M}}\dot{\mathbf{W}}+\mathbf{W}^T\bar{\mathbf{C}}\mathbf{W},\\ \mathbf{N}&=\mathbf{W}^T\bar{\mathbf{N}}.\end{aligned}$$ □

Note that the above model relates the active joint torques $\boldsymbol{\tau}_\mathbf{a}$ and the end–effector coordinates $\mathbf{X}$. The inertia matrix $\mathbf{M}$ and the Coriolis matrix $\mathbf{C}$ satisfy the following structural properties as long as matrix $\mathbf{W}$ has full rank

Property 1. Matrix $\mathbf{M}$ is a symmetric and positive definite.

Property 2. Matrix $\dot{\mathbf{M}}-2\mathbf{C}$ is skew-symmetric.

Property 3. There exists a positive constant k_{C1} such that

$$\|\mathbf{C}\| \leq k_{\mathbf{C}1}\|\dot{\mathbf{X}}\|. \tag{29}$$

3. Model of the vision system

Consider the redundant planar parallel robot described previously together with its Cartesian coordinate frame $x_\mathbf{R}-y_\mathbf{R}$ (see Fig. 6). This coordinate frame defines a plane where the motion of the robot end-effector takes place. A camera providing an image of the whole robot workspace, including the robot end-effector, is perpendicular to the plane where the robot evolves. The optical center is located at a distance z with respect to the $x_\mathbf{R}-y_\mathbf{R}$ plane, and the intersection $\mathbf{O}=[O_x \;\; O_y]^T$ between the optical axis and the robot workspace is located anywhere in the robot workspace. Variable β denotes the orientation of the camera around the optical axis with respect to the negative side of axis $x_\mathbf{R}$ of the robot coordinate frame, measured clockwise.

The camera sensor has associated a coordinate frame called the image coordinate frame with axes x_i and y_i; they are parallel to the robot coordinate frame. The camera sensor captures the image that is later stored in the computer frame buffer and displayed in the computer screen. The visual feature of interest is the robot end-effector position $\mathbf{X_i}=[x_i \;\; y_i]^T$ defined in the image coordinate frame; the units for $\mathbf{X_i}$ are pixels. Image-processing algorithms, allow the estimation of the coordinate $\mathbf{X_i}$. Thus, this estimate feeds the control algorithm without further processing. This later feature is common to all image-based Visual Servoing algorithms and permits avoiding camera calibration procedures.

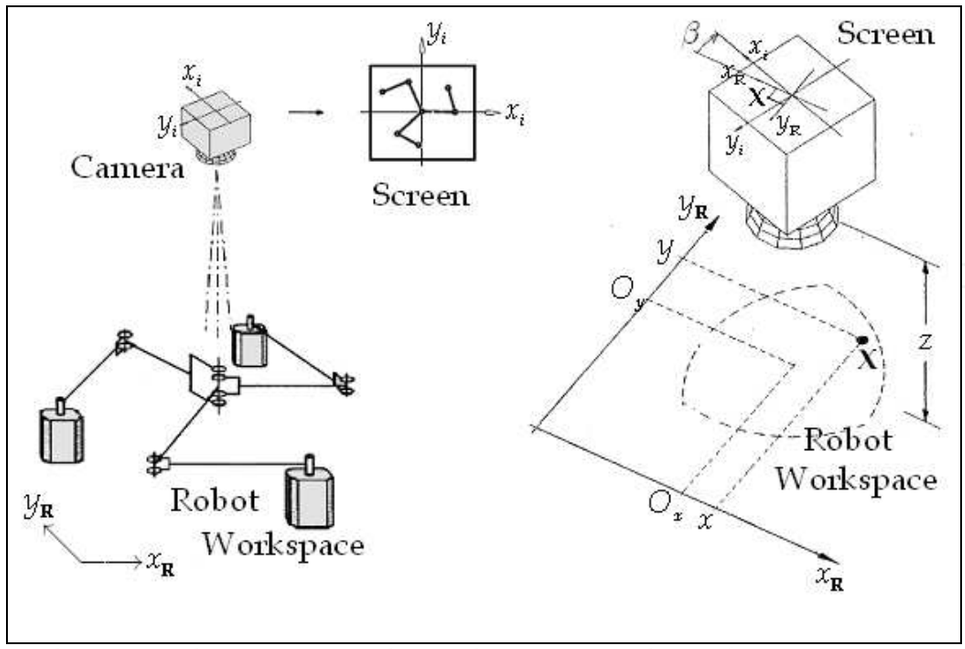

Fig. 6. Fixed-camera robotic system, robot and camera coordinate frames.

Let assume a perspective transformation as an ideal pinhole camera model (Kelly, 1996), the next relationship describes the position of the end-effector given in the image coordinate frame in terms of its position in the robot workspace

$$\mathbf{X}_{\mathrm{i}}=\eta h\mathbf{R}(\beta)(\mathbf{X}-\mathbf{O})+\mathbf{C}_{\mathrm{i}} \tag{30}$$

Parameter $\mathbf{C}_{\mathrm{i}}=\begin{bmatrix}C_{\mathrm{ix}} & C_{\mathrm{iy}}\end{bmatrix}^{T}$ is the image center, η is a scale factor in *pixels/m*, which is assumed negative, h is the magnification factor defined as

$$h=\frac{\lambda}{\lambda-z}<0 \tag{31}$$

where λ is the camera focal distance. $\mathbf{R}(\beta)\in SO(2)$ is the rotation matrix generated by clockwise rotating the camera about its optical axis by β radians

$$\mathbf{R}(\beta)=\begin{bmatrix}\cos\beta & -\sin\beta\\ \sin\beta & \cos\beta\end{bmatrix}. \tag{32}$$

The time derivative of (30) gives the end-effector linear velocity in terms of the image coordinate frame

$$\dot{\mathbf{X}}_{\mathrm{i}}=\eta h\mathbf{R}(\beta)\dot{\mathbf{X}}. \tag{33}$$

The following equation gives the desired end-effector position $\mathbf{X}^* = \begin{bmatrix} x^* & y^* \end{bmatrix}^T$ expressed in terms of the image coordinate frame

$$\mathbf{X}_\mathbf{i}^* = \eta h \mathbf{R}(\beta)(\mathbf{X}^* - \mathbf{O}) + \mathbf{C}_\mathbf{i} \tag{34}$$

where $\mathbf{X}^* = \begin{bmatrix} x^* & y^* \end{bmatrix}^T$ denotes the desired end-effector position expressed in the robot coordinate frame and located strictly inside the robot workspace, so there exists at least one (unknown) constant joint position vector, say $\mathbf{q}_\mathbf{d} \in \mathbb{R}^6$ for which the robot end-effector reaches the desired position, in other words, there exists a nonempty set $Q \subset \mathbb{R}^n$ such that $\mathbf{X}^* = f(\mathbf{q}_\mathbf{da}) \in \Omega$ for $\mathbf{q}_\mathbf{da} \in Q$. At this point, it is convenient to introduce the definition of the image position error $\tilde{\mathbf{X}}_\mathbf{i}$ as the visual distance between the measured and desired end-effector positions, see Fig. 7, i.e.

$$\tilde{\mathbf{X}}_\mathbf{i} = \mathbf{X}_\mathbf{i}^* - \mathbf{X}_\mathbf{i} = \begin{bmatrix} x_\mathbf{i}^* \\ y_\mathbf{i}^* \end{bmatrix} - \begin{bmatrix} x_\mathbf{i} \\ y_\mathbf{i} \end{bmatrix}. \tag{35}$$

Therefore, expressions (30),(34), and (35) allow defining the image error vector $\tilde{\mathbf{X}}_\mathbf{i}$ as

$$\tilde{\mathbf{X}}_\mathbf{i} = \eta h \mathbf{R}(\beta)[\varphi(\mathbf{q}_\mathbf{da}) - \varphi(\mathbf{q}_\mathbf{a})]. \tag{36}$$

Assuming a fixed desired position, taking the time derivative of the image position error yields

$$\frac{d\tilde{\mathbf{X}}_\mathbf{i}}{dt} = -\dot{\mathbf{X}}_\mathbf{i} = -\eta h \mathbf{R}(\beta)\dot{\mathbf{X}}. \tag{37}$$

4. Visual PID control algorithm

4.1 Preliminaries

A standard linear PID control law has the following form

$$u = K_P e + K_I \int_0^t e(\sigma)d\sigma + K_D \dot{e} \tag{38}$$

Here, variable $e = r - y$ defines the error with r the set point and y the output variable; therefore, the error e as well as its time-integral and time-derivative feed this algorithm. In some cases, the time derivative $-\dot{y}$ replaces $\dot{e}$ leading to the controller

$$u = K_P e + K_I \int_0^t e(\sigma)d\sigma - K_D \dot{y} \tag{39}$$

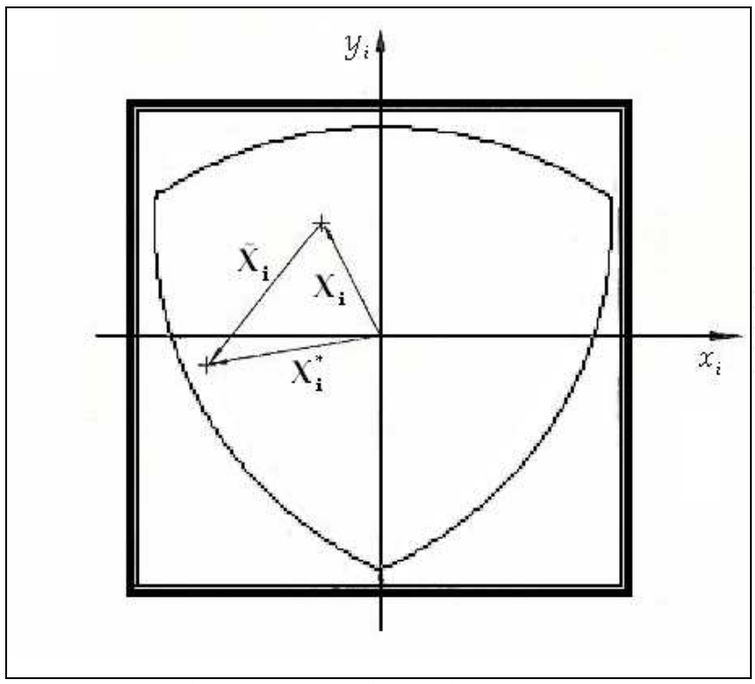

Fig. 7. Image position error in the image coordinate frame.

This last controller attenuates overshoots in face of abrupt changes in the set point value. When applied to joint control of robot manipulators, the linear PID controller leads to local stability or semi-global stability results. Applying a saturating function to the error, the Authors in references (Kelly, 1998) and (Santibañez & Kelly, 1998) were able to obtain global stability results. The next expression is an example of a PID controller using saturating functions

$$u = K_P e + K_I \int_0^t f(e(\sigma))d\sigma - K_D \dot{y}. \tag{40}$$

In this case, the term $f(\cdot)$ corresponds to a saturation function applied to the error. The proposed method for the control the redundant parallel robot will resort on a similar approach. The following definition states some key properties of the saturating functions used in the control law described in subsequent paragraphs.

***Definition** 1.* $\mathcal{F}(m,\varepsilon,\mathbf{x})$ with $1 \geq m > 0$, $\varepsilon > 0$ and $\mathbf{x} \in \mathbb{R}^n$ denotes the set of all continuous differentiable increasing functions $f(\mathbf{x}) = [f(x_1) \quad f(x_2) \quad \cdots \quad f(x_n)]^T$ such that

- $|x| \geq |f(x)| \geq m|x|, \quad \forall\, x \in \mathbb{R} : |x| < \varepsilon;$
- $\varepsilon \geq |f(x)| \geq m\varepsilon, \quad \forall\, x \in \mathbb{R} : |x| \geq \varepsilon;$
- $1 \geq (d/dx) f(x) \geq 0;$

where $|\cdot|$ stands for the absolute value.

Figure 8 depicts the region allowed for functions belonging to the set $\mathcal{F}(m,\varepsilon,\mathbf{x})$. Two important properties of functions $f(\mathbf{x})$ belonging to $\mathcal{F}(m,\varepsilon,\mathbf{x})$ are now stated

Property 4. The Euclidean norm of $f(\mathbf{x}), \mathbf{x}\in\mathbb{R}^n$ satisfies

$$\|f(\mathbf{x})\|\geq\begin{cases} m\|\mathbf{x}\|, & if\ \|\mathbf{x}\|<\varepsilon \\ m\varepsilon, & if\ \|\mathbf{x}\|\geq\varepsilon \end{cases},$$

$$\|f(\mathbf{x})\|\leq\begin{cases} \|\mathbf{x}\|, & if\ \|\mathbf{x}\|<\varepsilon \\ \sqrt{n}\varepsilon, & if\ \|\mathbf{x}\|\geq\varepsilon. \end{cases}$$

Property 5. The function $f(\mathbf{x})^T\mathbf{x}$, $\mathbf{x}\in\mathbb{R}^n$ satisfies

$$f(\mathbf{x})^T\mathbf{x}\geq\begin{cases} m\|\mathbf{x}\|^2, & if\ \ \|\mathbf{x}\|<\varepsilon \\ m\varepsilon\|\mathbf{x}\|, & if\ \ \|\mathbf{x}\|\geq\varepsilon. \end{cases}$$

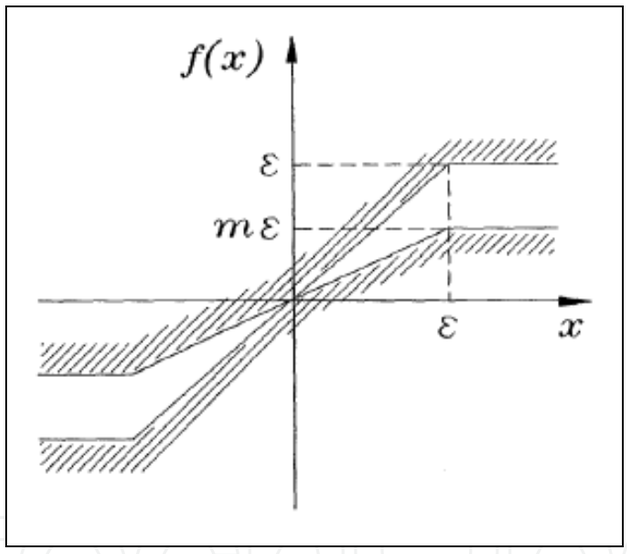

Fig. 8. Saturating functions $\mathcal{F}(m,\varepsilon,\mathbf{x})$.

4.2 Control problem formulation

Consider the robotic system described in Fig.6. Assume that the camera together with the vision system provide the position $\mathbf{X}_i=[x_i\ y_i]^T$ of the robot end-effector expressed in the image coordinate frame. Suppose that measurements of joint position $\mathbf{q}$ and velocity $\dot{\mathbf{q}}$ are available. However, the magnification factor h and the position of the intersection of the camera axis with the robot workspace $\mathbf{O}=[O_x\ O_y]^T$ expressed in terms of the robot coordinate frame are assumed unknown. The control problem can be stated as that of designing a control law for the active joint actuator torques $\boldsymbol{\tau}_a$ such that the robot end-

effector reaches, in the image supplied on the screen, the desired position defined in the robot workspace, i.e., the control law must ensure that $\lim_{t\to\infty}(\mathbf{X}_\mathbf{i}^* - \mathbf{X}_\mathbf{i}) = \mathbf{0}$ for $\mathbf{X}_\mathbf{i}^* \in \Omega \subset \mathbb{R}^2$.

In order to solve the problem stated previously, assume that

$$\mathbf{S}^T \boldsymbol{\tau}_\mathbf{a} = \mathbf{u}. \tag{41}$$

Variable $\mathbf{u}$ defines a control signal in terms of the end-effector coordinates, and drives the robot dynamics (28). Hence, torques $\boldsymbol{\tau}_\mathbf{a}$ are the solutions of the following equation

$$\boldsymbol{\tau}_\mathbf{a} = (\mathbf{S}^T)^\dagger \mathbf{u}. \tag{42}$$

The symbol $(\mathbf{S}^T)^\dagger = \mathbf{S}(\mathbf{S}^T\mathbf{S})^{-1}$ stands for the Moore-Penrose pseudo-inverse of $\mathbf{S}^T$, satisfying $\mathbf{S}^T(\mathbf{S}^T)^\dagger = I$, and $\left[\mathbf{S}^T(\mathbf{S}^T)^\dagger\right]^T = \mathbf{S}^\dagger\mathbf{S} = I$. Solution (42) makes sense only if the pseudo-inverse $(\mathbf{S}^T)^\dagger$ is well defined, i.e., if matrix $\mathbf{S}$ has full rank. Matrix $\mathbf{S}$ loose rank if the parallel robot reaches a singular configuration; in the sequel, matrix $\mathbf{S}$ is assumed full rank. Let us propose the following PID control law

$$\mathbf{u} = \mathbf{K}_\mathbf{P}\mathbf{Y} + \mathbf{K}_\mathbf{I}\int_0^t f(\mathbf{Y}(\sigma))d\sigma - \mathbf{K}_\mathbf{D}\dot{\mathbf{X}} \tag{43}$$

Using (41) and (42) allows writing the control law (39) as follows

$$\boldsymbol{\tau}_\mathbf{a} = (\mathbf{S}^T)^\dagger\left[\mathbf{K}_\mathbf{P}\mathbf{Y} + \mathbf{K}_\mathbf{I}\int_0^t f(\mathbf{Y}(\sigma))d\sigma - \mathbf{K}_\mathbf{D}\dot{\mathbf{X}}\right] \tag{44}$$

The term $\mathbf{Y} = \mathbf{R}(\beta)^T\tilde{\mathbf{X}}_\mathbf{i}$ corresponds to the rotated position error, variables $\mathbf{K}_\mathbf{P}$, $\mathbf{K}_\mathbf{I}$ and $\mathbf{K}_\mathbf{D}$ are diagonal positive definite matrices and correspond to the proportional, integral and derivative actions. The above control law is composed of a linear Proportional Derivative (PD) term plus an integral action of the nonlinear function of the position error $f(\mathbf{Y})$. Note that the position error $\tilde{\mathbf{X}}_\mathbf{i}$ feeds the proportional and the integral actions, whereas the active joint velocities $\dot{\mathbf{q}}_\mathbf{a}$ feed the derivative action using the relationship $\dot{\mathbf{X}} = \mathbf{S}^\dagger\dot{\mathbf{q}}_\mathbf{a}$. Note also that in order to implement control law (44) it is not necessary to know the parameters η and h; hence, camera calibration is not necessary. The Fig. 9 depicts the corresponding block diagram.

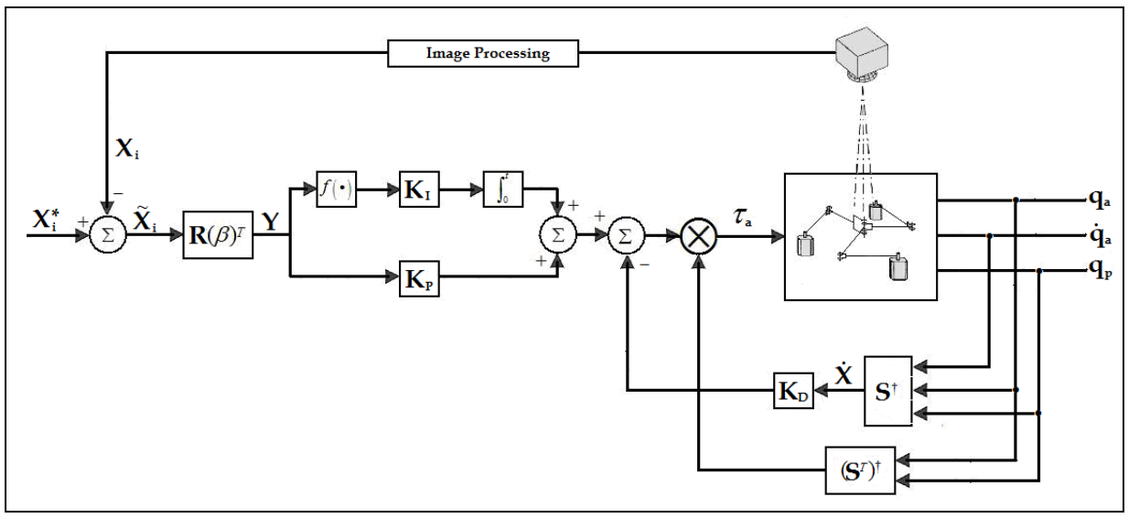

Fig. 9. Block diagram of the Visual PID control law.

Substituting control law (44) into the robot dynamics (28) and defining an auxiliary variable $\mathbf{Z}$ as

$$\mathbf{Z}=\int_0^t f(\mathbf{Y}(\sigma))d\sigma-\mathbf{K}_\mathbf{I}^{-1}\mathbf{N} \tag{45}$$

yield the closed-loop dynamics

$$\frac{d}{dt}\begin{bmatrix}\mathbf{Y}\\ \dot{\mathbf{X}}\\ \mathbf{Z}\end{bmatrix}=\begin{bmatrix}-\eta h\dot{\mathbf{X}}\\ \mathbf{M}^{-1}\{\mathbf{K}_\mathbf{P}\mathbf{Y}+\mathbf{K}_\mathbf{I}\mathbf{Z}-\mathbf{K}_\mathbf{D}\dot{\mathbf{X}}-\mathbf{C}\dot{\mathbf{X}}\}\\ f(\mathbf{Y})\end{bmatrix} \tag{46}$$

The following proposition provides conditions on the controller gains $\mathbf{K}_\mathbf{P}, \mathbf{K}_\mathbf{D}$, and $\mathbf{K}_\mathbf{I}$ guaranteeing the asymptotic stability of the equilibrium of the closed-loop dynamics.

Proposition 2. Consider the robot dynamics (28) together with control law (44) where $f(\mathbf{Y})\in\mathcal{F}(m,\varepsilon,x)$. Assume that the PID controller gains fulfill

$$\lambda_{\min}\{\mathbf{K}_\mathbf{D}\}>\lambda_{\max}\{\mathbf{M}\}+k_{C2},\ k_{C2}>0 \tag{47}$$

$$\lambda_{\min}\{\mathbf{K}_\mathbf{P}\}>\lambda_{\max}\{\mathbf{K}_\mathbf{I}\}+\frac{2}{\eta h}\lambda_{\max}\{\mathbf{M}\} \tag{48}$$

Then, the equilibrium $\begin{bmatrix}\mathbf{Y} & \dot{\mathbf{X}} & \mathbf{Z}\end{bmatrix}^T=\begin{bmatrix}0 & 0 & 0\end{bmatrix}^T$ of (46) is asymptotically stable.

***Proof of Proposition 2*:** The stability analysis employs the following Lyapunov Function Candidate

$$V(\mathbf{Y},\dot{\mathbf{X}},\mathbf{Z})=\frac{1}{2}\left[\dot{\mathbf{X}}-\frac{1}{\eta h}f(\mathbf{Y})\right]^{T}\mathbf{M}\left[\dot{\mathbf{X}}-\frac{1}{\eta h}f(\mathbf{Y})\right]+\frac{1}{2\eta h}[\mathbf{Z}+\mathbf{Y}]^{T}\mathbf{K}_{\mathbf{I}}[\mathbf{Z}+\mathbf{Y}]+\frac{1}{\eta^{2}h^{2}}\int_{0}^{\mathbf{Y}}f(w)^{T}\mathbf{K}_{\mathbf{D}}dw$$
$$+\frac{1}{2\eta h}\mathbf{Y}^{T}[\mathbf{K}_{\mathbf{P}}-\mathbf{K}_{\mathbf{I}}]\mathbf{Y}-\frac{1}{2\eta^{2}h^{2}}f(\mathbf{Y})^{T}\mathbf{M}f(\mathbf{Y}). \tag{49}$$

The first term is a nonnegative function of $\mathbf{Y}$ and $\dot{\mathbf{X}}$, while the second is a nonnegative function of variables $\mathbf{Y}$ and $\mathbf{Z}$. Using the fact that $\mathbf{K}_{\mathbf{D}}$ is a diagonal positive definite matrix, $f(\mathbf{0})=\mathbf{0}$, and the entries of $f(\mathbf{Y})$ are increasing functions, it is not difficult to show that the third term satisfies

$$\frac{1}{\eta^{2}h^{2}}\int_{0}^{\mathbf{Y}}f(w)^{T}\mathbf{K}_{\mathbf{D}}dw>0,\ \forall\ \mathbf{Y}\neq 0 \tag{50}$$

Therefore, this term is positive definite with respect to $\mathbf{Y}$. For the remaining terms, notice that using the Rayleigh-Ritz inequality leads to

$$\frac{1}{2\eta h}\mathbf{Y}^{T}[\mathbf{K}_{\mathbf{P}}-\mathbf{K}_{\mathbf{I}}]\mathbf{Y}-\frac{1}{2\eta^{2}h^{2}}f(\mathbf{Y})^{T}\mathbf{M}f(\mathbf{Y})\geq\frac{1}{2\eta h}\left[\lambda_{\min}\{\mathbf{K}_{\mathbf{P}}\}-\lambda_{\max}\{\mathbf{K}_{\mathbf{I}}\}\right]\|\mathbf{Y}\|^{2}-\frac{1}{2\eta^{2}h^{2}}\lambda_{\max}\{\mathbf{M}\}\|f(\mathbf{Y})\|^{2}.$$

The above result and Property 4 yields

$$\frac{1}{2\eta h}\left[\lambda_{\min}\{\mathbf{K}_{\mathbf{P}}\}-\lambda_{\max}\{\mathbf{K}_{\mathbf{I}}\}\right]\|\mathbf{Y}\|^{2}-\frac{1}{2\eta^{2}h^{2}}\lambda_{\max}\{\mathbf{M}\}\|f(\mathbf{Y})\|^{2}\geq\begin{cases}\frac{1}{2\eta h}\left[\lambda_{\min}\{\mathbf{K}_{\mathbf{P}}\}-\lambda_{\max}\{\mathbf{K}_{\mathbf{I}}\}-\frac{1}{\eta h}\lambda_{\max}\{\mathbf{M}\}\right]\|\mathbf{Y}\|^{2}, & if\ \|\mathbf{Y}\|<\varepsilon\\ \frac{1}{2\eta h}\left[\lambda_{\min}\{\mathbf{K}_{\mathbf{P}}\}-\lambda_{\max}\{\mathbf{K}_{\mathbf{I}}\}-\frac{2}{\eta h}\lambda_{\max}\{\mathbf{M}\}\right]\varepsilon^{2}, & if\ \|\mathbf{Y}\|\geq\varepsilon.\end{cases} \tag{51}$$

The right-hand side of (51) is a positive definite function with respect to $\mathbf{Y}$ because of inequality (48); therefore, the Lyapunov function candidate (49) is a positive definite function. The following equation gives the time derivative of Lyapunov Function Candidate (49)

$$\frac{d}{dt}V(\mathbf{Y},\dot{\mathbf{X}},\mathbf{Z})=\dot{\mathbf{X}}^{T}\mathbf{M}\ddot{\mathbf{X}}-\frac{1}{\eta h}\dot{\mathbf{X}}^{T}\mathbf{M}\dot{f}(\mathbf{Y})-\frac{1}{\eta h}f(\mathbf{Y})^{T}\mathbf{M}\ddot{\mathbf{X}}+\frac{1}{\eta^{2}h^{2}}f(\mathbf{Y})^{T}\mathbf{M}\dot{f}(\mathbf{Y})+\frac{1}{2}\dot{\mathbf{X}}^{T}\dot{\mathbf{M}}\dot{\mathbf{X}}-\frac{1}{\eta h}f(\mathbf{Y})^{T}\dot{\mathbf{M}}\dot{\mathbf{X}}+\frac{1}{2\eta^{2}h^{2}}f(\mathbf{Y})^{T}\dot{\mathbf{M}}f(\mathbf{Y})$$
$$+\frac{1}{\eta h}\mathbf{Z}^{T}\mathbf{K}_{\mathbf{I}}\dot{\mathbf{Z}}+\frac{1}{\eta h}\mathbf{Z}^{T}\mathbf{K}_{\mathbf{I}}\dot{\mathbf{Y}}+\frac{1}{\eta h}\mathbf{Y}^{T}\mathbf{K}_{\mathbf{I}}\dot{\mathbf{Z}}+\frac{1}{\eta h}\mathbf{Y}^{T}\mathbf{K}_{\mathbf{I}}\dot{\mathbf{Y}}+\frac{d}{dt}\left[\frac{1}{\eta^{2}h^{2}}\int_{0}^{\mathbf{Y}}f(w)^{T}\mathbf{K}_{\mathbf{D}}dw\right]+\frac{1}{\eta h}\mathbf{Y}^{T}\mathbf{K}_{\mathbf{P}}\dot{\mathbf{Y}}-\frac{1}{\eta h}\mathbf{Y}^{T}\mathbf{K}_{\mathbf{I}}\dot{\mathbf{Y}}$$
$$-\frac{1}{\eta^{2}h^{2}}f(\mathbf{Y})^{T}\mathbf{M}\dot{f}(\mathbf{Y})-\frac{1}{2\eta^{2}h^{2}}f(\mathbf{Y})^{T}\dot{\mathbf{M}}f(\mathbf{Y}).$$

Applying the Leibnitz rule to the time derivative of the integral term produces

$$\frac{d}{dt}\left[\frac{1}{\eta^{2}h^{2}}\int_{0}^{\mathbf{Y}}f(w)^{T}\mathbf{K}_{\mathbf{D}}dw\right]=\frac{1}{\eta^{2}h^{2}}f(\mathbf{Y})^{T}\mathbf{K}_{\mathbf{D}}\dot{\mathbf{Y}}.$$

From the above, the Lyapunov Functions Candidate time derivative becomes

$$\frac{d}{dt}V(\mathbf{Y},\dot{\mathbf{X}},\mathbf{Z})=\dot{\mathbf{X}}^T\mathbf{M}\ddot{\mathbf{X}}-\frac{1}{\eta h}\dot{\mathbf{X}}^T\mathbf{M}\dot{f}(\mathbf{Y})-\frac{1}{\eta h}f(\mathbf{Y})^T\mathbf{M}\ddot{\mathbf{X}}+\frac{1}{2}\dot{\mathbf{X}}^T\dot{\mathbf{M}}\dot{\mathbf{X}}-\frac{1}{\eta h}f(\mathbf{Y})^T\dot{\mathbf{M}}\dot{\mathbf{X}}$$
$$+\frac{1}{\eta h}\mathbf{Z}^T\mathbf{K}_\mathbf{I}\dot{\mathbf{Z}}+\frac{1}{\eta h}\mathbf{Z}^T\mathbf{K}_\mathbf{I}\dot{\mathbf{Y}}+\frac{1}{\eta h}\mathbf{Y}^T\mathbf{K}_\mathbf{I}\dot{\mathbf{Z}}+\frac{1}{\eta h}\mathbf{Y}^T\mathbf{K}_\mathbf{I}\dot{\mathbf{Y}}+\frac{1}{\eta^2h^2}f(\mathbf{Y})^T\mathbf{K}_\mathbf{D}\dot{\mathbf{Y}}+\frac{1}{\eta h}\mathbf{Y}^T\mathbf{K}_\mathbf{P}\dot{\mathbf{Y}}-\frac{1}{\eta h}\mathbf{Y}^T\mathbf{K}_\mathbf{I}\dot{\mathbf{Y}} \tag{52}$$

Note that the time derivative of the saturating function $f(\mathbf{Y})$ fulfills $\dot{f}(\mathbf{Y})=-\eta hF(\mathbf{Y})\ddot{\mathbf{X}}$. The term $F(\mathbf{Y})$ is a diagonal matrix, and its entries $\partial f(\mathbf{Y}_j)/\partial\mathbf{Y}_j;\ j=1,2$ are nonnegative and smaller than or equal to one. Substituting the closed-loop dynamics (46) into (52) yields

$$\frac{d}{dt}V(\mathbf{Y},\dot{\mathbf{X}},\mathbf{Z})=\dot{\mathbf{X}}^T\mathbf{K}_\mathbf{P}\mathbf{Y}+\dot{\mathbf{X}}^T\mathbf{K}_\mathbf{I}\mathbf{Z}-\dot{\mathbf{X}}^T\mathbf{K}_\mathbf{D}\dot{\mathbf{X}}-\dot{\mathbf{X}}^T\mathbf{C}\dot{\mathbf{X}}+\dot{\mathbf{X}}^T\mathbf{M}F(\mathbf{Y})\ddot{\mathbf{X}}$$
$$-\frac{1}{\eta h}f(\mathbf{Y})^T\mathbf{K}_\mathbf{P}\mathbf{Y}-\frac{1}{\eta h}f(\mathbf{Y})^T\mathbf{K}_\mathbf{I}\mathbf{Z}+\frac{1}{\eta h}f(\mathbf{Y})^T\mathbf{K}_\mathbf{D}\dot{\mathbf{X}}+\frac{1}{\eta h}f(\mathbf{Y})^T\mathbf{C}\dot{\mathbf{X}}+\frac{1}{2}\dot{\mathbf{X}}^T\dot{\mathbf{M}}\dot{\mathbf{X}}-\frac{1}{\eta h}f(\mathbf{Y})^T\dot{\mathbf{M}}\dot{\mathbf{X}}$$
$$+\frac{1}{\eta h}\mathbf{Z}^T\mathbf{K}_\mathbf{I}f(\mathbf{Y})-\mathbf{Z}^T\mathbf{K}_\mathbf{I}\dot{\mathbf{X}}+\frac{1}{\eta h}\mathbf{Y}^T\mathbf{K}_\mathbf{I}f(\mathbf{Y})-\mathbf{Y}^T\mathbf{K}_\mathbf{I}\dot{\mathbf{X}}-\frac{1}{\eta h}f(\mathbf{Y})^T\mathbf{K}_\mathbf{D}\dot{\mathbf{X}}-\mathbf{Y}^T\mathbf{K}_\mathbf{P}\dot{\mathbf{X}}+\mathbf{Y}^T\mathbf{K}_\mathbf{I}\dot{\mathbf{X}}.$$

Some simplifications and the use of *Property 2* lead to the following expression for the time derivative of the Lyapunov Function Candidate (49) along the trajectories of the closed-loop system (46)

$$\dot{V}(\mathbf{Y},\dot{\mathbf{X}},\mathbf{Z})=-\dot{\mathbf{X}}^T[\mathbf{K}_\mathbf{D}-\mathbf{M}F(\mathbf{Y})]\ddot{\mathbf{X}}-\frac{1}{\eta h}f(\mathbf{Y})^T[\mathbf{K}_\mathbf{P}-\mathbf{K}_\mathbf{I}]\mathbf{Y}-\frac{1}{\eta h}f(\mathbf{Y})^T\mathbf{C}^T\dot{\mathbf{X}} \tag{53}$$

By using *Properties 3* and *4* we have

$$-\frac{1}{\eta h}f(\mathbf{Y})^T\mathbf{C}^T\dot{\mathbf{X}}\le\frac{1}{\eta h}k_{\mathrm{C1}}\sqrt{2}\varepsilon\|\dot{\mathbf{X}}\|^2=k_{\mathrm{C2}}\|\dot{\mathbf{X}}\|^2.$$

On the other hand, note that

$$\dot{\mathbf{X}}^T\mathbf{M}F(\mathbf{Y})\ddot{\mathbf{X}}\le\lambda_{\max}\{\mathbf{M}\}\|\dot{\mathbf{X}}\|^2.$$

Therefore, the time derivative of the Lyapunov Function Candidate (53) satisfies

$$\dot{V}(\mathbf{Y},\dot{\mathbf{X}},\mathbf{Z})\le-\gamma\|\dot{\mathbf{X}}\|^2-\frac{1}{\eta h}f(\mathbf{Y})^T[\mathbf{K}_\mathbf{P}-\mathbf{K}_\mathbf{I}]\mathbf{Y} \tag{54}$$

The parameter $\gamma=\lambda_{\min}\{\mathbf{K}_\mathbf{D}\}-\lambda_{\max}\{\mathbf{M}\}-k_{\mathrm{C2}}$ is positive because of the selection of $\mathbf{K}_\mathbf{D}$ in (47). The fact that $\mathbf{K}_\mathbf{P}$ and $\mathbf{K}_\mathbf{I}$ are diagonal positive definite matrices and $\mathbf{Y}_i f(\mathbf{Y}_i)\ge 0$ allows establishing the following upper bound for the second term of (54)

$$-\frac{1}{\eta h}f(\mathbf{Y})^T[\mathbf{K}_\mathbf{P}-\mathbf{K}_\mathbf{I}]\mathbf{Y}\le-\frac{1}{\eta h}[\lambda_{\min}\{\mathbf{K}_\mathbf{P}\}-\lambda_{\max}\{\mathbf{K}_\mathbf{I}\}]f(\mathbf{Y})^T\mathbf{Y}.$$

Taking into account *Property 5* leads to

$$-\frac{1}{\eta h} f(\mathbf{Y})^T [\mathbf{K_P} - \mathbf{K_I}] \mathbf{Y} \leq \begin{cases} -\mu \|\mathbf{Y}\|^2, & if \ \|\mathbf{Y}\| < \varepsilon \\ -\mu\varepsilon \|\mathbf{Y}\|, & if \ \|\mathbf{Y}\| \geq \varepsilon \end{cases} \tag{55}$$

The choice of $\mathbf{K_P}$ in (48) ensures $\mu = \frac{m}{\eta h}[\lambda_{\min}\{\mathbf{K_P}\} - \lambda_{\max}\{\mathbf{K_I}\}] > 0$.

Therefore, incorporating (55) into(54) produces the following a negative semi-definite function

$$\dot{V}(\mathbf{Y}, \dot{\mathbf{X}}, \mathbf{Z}) \leq \begin{cases} -\gamma \|\dot{\mathbf{X}}\|^2 - \mu \|\mathbf{Y}\|^2, & if \ \|\mathbf{Y}\| < \varepsilon \\ -\gamma \|\dot{\mathbf{X}}\|^2 - \mu\varepsilon \|\mathbf{Y}\|, & if \ \|\mathbf{Y}\| \geq \varepsilon \end{cases} \tag{56}$$

Using the fact that the Lyapunov Function Candidate (49) is a positive definite function and its time derivative is a negative semi-definite function, allows concluding that the equilibrium of the closed-loop system (46) is stable. Finally, by invoking the LaSalle's invariance principle permits establishing asymptotical stability as follows. Since $\dot{V}(\mathbf{Y}, \dot{\mathbf{X}}, \mathbf{Z}) \equiv 0$ if and only if $\dot{\mathbf{X}}$ and $\mathbf{Y}$ are zero. This implies that $\ddot{\mathbf{X}}$, $\dot{\mathbf{Y}}$, and $f(\mathbf{Y})$ are also zero; then, from the closed-loop system (46) , it follows that $\mathbf{M}^{-1}\{\mathbf{K_P}\mathbf{Y} + \mathbf{K_I}\mathbf{Z} - \mathbf{K_D}\dot{\mathbf{X}} - \mathbf{C}\dot{\mathbf{X}}\} = \mathbf{0}$. This result allows concluding $\mathbf{K_I}\mathbf{Z} = 0$. Therefore, $\mathbf{Z} = 0$ because $\mathbf{K_I}$ is a diagonal positive definite matrix. Thus, $\dot{V}(\mathbf{Y}, \dot{\mathbf{X}}, \mathbf{Z}) \equiv 0$ in the invariant set $\{\mathbf{Y} = \mathbf{0}, \dot{\mathbf{X}} = \mathbf{0}, \mathbf{Z} = \mathbf{0}\}$ and asymptotic stability follows.

□

Some comments regarding the proposed control law are worth making. Firstly, note that the measurements provided by the vision system feed the integral and proportional actions. The Derivative action employs velocity measurements from the active joints; then, using the relationship $\dot{\mathbf{X}} = \mathbf{S}^{\dagger}\dot{\mathbf{q}}_{\mathbf{a}}$ allows obtaining velocity estimates of the robot end effector. In practice, since in most cases, the robot active joints are endowed only with position sensors, high-pass filter or backward differences approaches would permit estimating $\dot{\mathbf{q}}_{\mathbf{a}}$ from position measurements. An advantage of using $\dot{\mathbf{q}}_{\mathbf{a}}$ for generating the Derivative action is that position measurements at the active joints, supplied in most cases by optical encoders, are obtained at higher sampling rates compared with the measurements provided by a vision system. The reader will note in the next section that the sampling rate for the incremental optical encoders associated to the active joints is five times faster than that corresponding to the measurements obtained though the vision system.

5. Experimental Results

Experiments conducted on a laboratory prototype (Fig. 10) display the performance of the proposed controller. The nominal link lengths of the prototype are $L = 15\ cm$. Brushed servomotors from Moog, model C34L80W40 drive the active joints. Incremental optical encoders attached to the motors provide position measurements corresponding to the vector $\mathbf{q}_{\mathbf{a}}$. These motors steer the active joints through timing belts with a 3.6:1 ratio. Pulse width modulation digital amplifiers from Copley

Controls, model Junus 90 and working in current mode, drive the motors. Absolute optical encoders from US Digital, model A2, with 4096 pulses per turn, supply measurements of the robot active and passive joints angles θ_i and α_i that allows computing the Jacobians $\mathbf{S}^{\dagger}$ and $(\mathbf{S}^{T})^{\dagger}$.

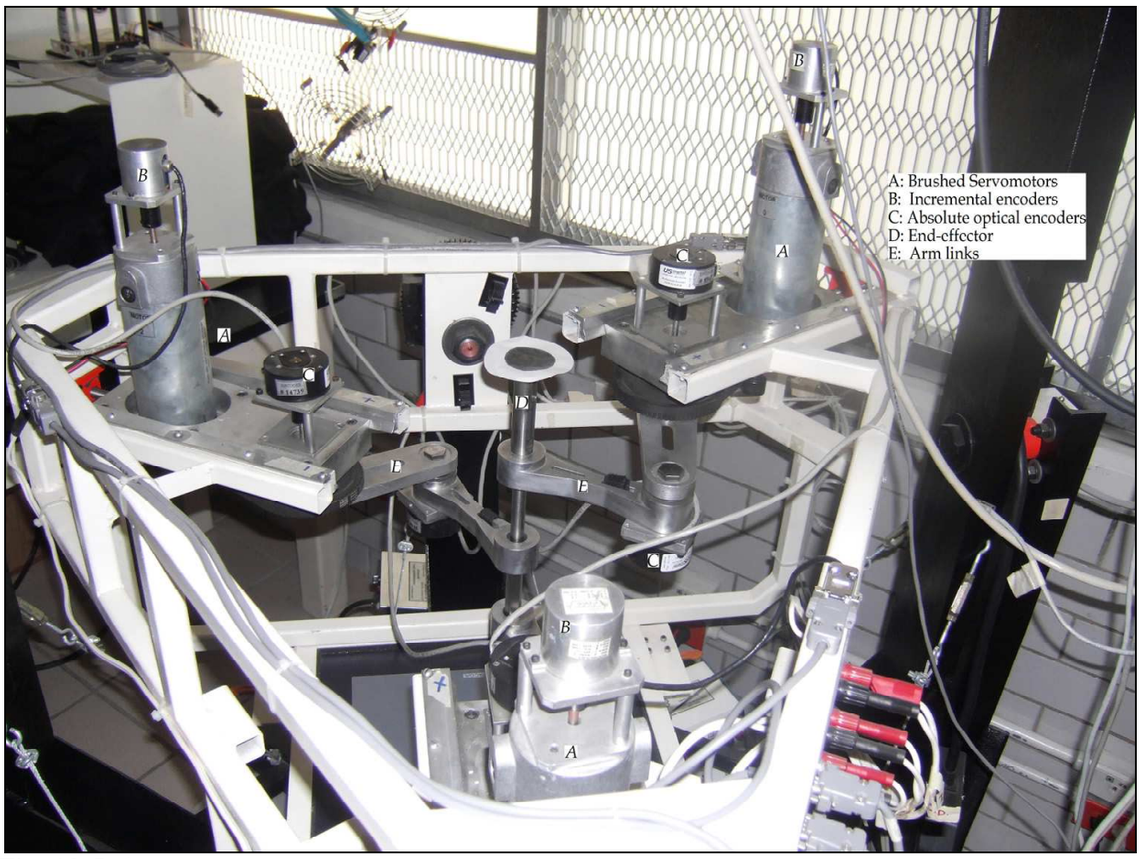

Fig. 10. Laboratory prototype.

Two computers compose the control architecture; which is an update of the architecture presented in (Soria et al. 2006). The first computer, called the vision computer and endowed with an Intel Core2 processor running at 2.4 GHz, executes image acquisition; a Dalsa Camera, model CA-1D-128A is connected to this computer by means of a National Instruments card, model NI-1422. Image processing is performed using Visual C++ and the DIAS software[1]. The second computer, called the control computer and endowed with an Intel 4 processor running at 3.0 GHz, executes the control algorithm and performs data logging. This computer receives data from the vision computer through an RS-232 port at 115 *Kbaud*. Data acquisition is carried out through a data card from Quanser consulting, model MultiQ 3. This card reads signals from the optical incremental encoders attached to the motors and supplies control voltages to the power amplifiers. Optical absolute encoders connect to the control computer through an RS-232 using an AD2-B adapter from US Digital.

Algorithms are coded using the Matlab/Simulink 5.2 software under the Wincon 3.02 real-time environment. A counter in the MultiQ 3 card sets a sampling period of

$T_{ie}=0.5ms$, which corresponds to the master clock of the closed-loop system; this sampling period also sets the sampling time for reading the active joint incremental optical encoders. The image sampling period is $T_{im}=5ms$; during this time interval, the vision computer executes data acquisition and processing; it also includes the time required to send the robot end-effector coordinates to the control computer through the RS-232 link. It is worth mentioning that T_{im} corresponds to the time delay introduced in the visual measurements. The absolute encoder measurements are sampled every $T_{ab}=15ms$. The sampling time for the visual and absolute encoder, measurements are synchronized with the master clock. The choice for the numerical method in Simulink was the ODE 45 Dormand-Price algorithm.

Gains for the proposed controller were set to $\mathbf{K_P}=diag\{0.22 \quad 0.22\}$, $\mathbf{K_D}=diag\{0.004 \quad 0.004\}$, and $\mathbf{K_I}=diag\{0.176 \quad 0.156\}$. The reference x_i^* is square wave of 16 pixels of amplitude, with a frequency of 0.2 Hz, while the reference y_i^* is a square wave with a frequency of 0.4 Hz. Fig 12 depicts the experimental position control results without and with integral action. The upper part in Fig. 12 corresponds to the x_i coordinate whereas the bottom part corresponds to the y_i coordinate. Fig.13 depicts the image position errors; note that when the reference changes, the position error settles around 0.5 pixels using the integral action. These results indicate that the integral action removes the steady state error without greatly affecting the transient response.

Fig. 11. Camera with image coordinate frame parallel to the robot coordinate frame.

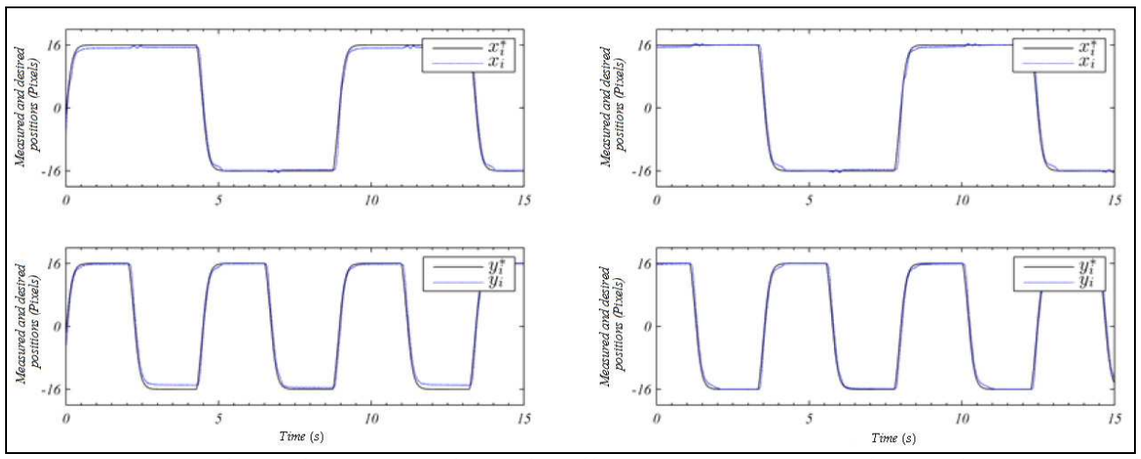

Fig. 12. Desired and measured end effector positions: Left, without integral action $\mathbf{K_I} = diag\{0 \quad 0\}$; right, with integral action $\mathbf{K_I} = diag\{0.176 \quad 0.156\}$.

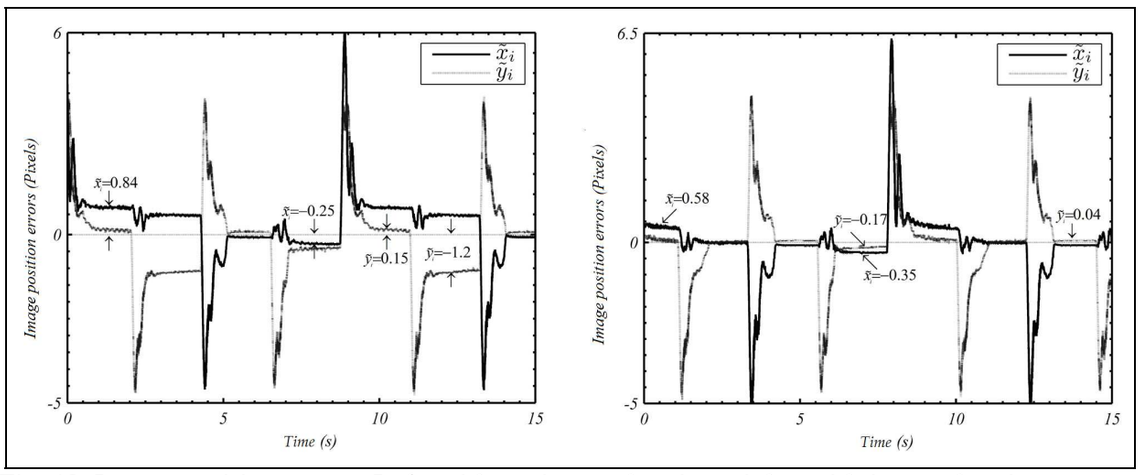

Fig. 13. Image position errors: Left, without integral action; right, with integral action.

6. Conclusion

This chapter has presented some modeling and control issues related to a class of overactuated planar parallel robots. After reviewing the kinematic and dynamic modeling of this kind of robots, the Authors propose a novel imaged-based Proportional-Integral-Derivative regulator. A key element in this control law is the measurement of the end-effector position using a vision system. This feature avoids using the robot Forward Kinematics employed traditionally for controlling planar parallel robots, and which requires an off-line calibration. Moreover, the proposed control law does not rely on camera calibration. A theoretical study provides conditions on the PID gains for obtaining asymptotic closed-loop stability. A practical implementation of the proposed method using a laboratory prototype shows a good performance of the closed-loop system. The experiments indicate that, as expected in a PID controller, the integral action removes the steady state error without a noticeable degradation in the transient response.

7. References

Angel, L.; Traslosheros, A.; Sebastian, J.M.; Pari, L.; Carelli, R. & Roberti, F. (2008). Vision-based control of the robotenis system, *Recent Progress in Robotics*, Springer Verlag. LNCIS 370, pp. 229-240.

Arimoto, S. & Miyazaki, F. (1984). Stability and robustness of PID feedback control for robot manipulators of sensory capability, In*: Robotics Research: First International Symposium*, Brady, M. & Paul, R. P., Ed. Cambridge, 783-799, MIT Press, MA.

Andreff, N. & Martinet, Ph. (2006). Unifying kinematic modeling, identification, and control of a Gough-Stewart parallel robot into a vision-based framework, *IEEE Trans. on Robotics*, Vol. 22, No. 6.

Andreff, N.; Dallej, T. & Martinet, Ph. (2007). Image-based Visual Servoing of a Gough-Stewart Parallel Manipulator using Leg Observations, *The International Journal of Robotic Research*, Vol. 26, pp. 667-687.

Chaumette, F. & Hutchinson, S. (2006). *Visual servo control part I: Basic approaches*. IEEE Robotics & Automation Magazine, December 2006.

Chaumette, F. & Hutchinson, S. (2007). *Visual servo control part II: Advanced approaches*. IEEE Robotics & Automation Magazine, March 2007.

Cheng, H.; Yiu, Y.K. & Li, Z. (2003). Dynamics and Control of Redundantly Actuated Parallel Manipulators, *IEEE/ ASME Transactions on Mechatronics*, Vol. 8, No. 4, December 2003, 483-491.

Corke, P. (1996). *Visual Control of Robots: High performance Visual Servoing*. Taunton, Somerset, England: Research Studies Press.

Dallej, T.; Andreff, N. & Martinet, Ph. (2007). Image-based visual servoing of the I4R parallel robot without propioceptive sensors. *Proceedings of the Int. Conf. on Robotics and Automation,* Roma, Italy.

Hutchinson, S.; Hager, G.D. & Corke P.I. (1996) A tutorial on visual servo control. *IEEE Transactions on Robotics and Automation*, Vol. 12, No. 5, October 1996, 651-670.

Kelly, R. (1995). A tuning procedure for stable PID control of robot manipulators, *Robotica*, pt. 2, Vol. 13, Mar. /Apr. 1995, pp. 141-148.

Kelly, R. (1996). Robust Asymptotically Stable Visual Servoing of Planar Robots, *IEEE Transactions on Robotics and Automation*, Vol. 12, No. 5, October 1996, 759-766.

Kelly, R. (1998). Global Positioning of Robot Manipulators via PD Control plus a Class of Nonlinear Integral Actions, *IEEE Transactions on Automatic Control*, Vol. 43, No. 7, July 1998, pp. 934-938.

Kock, S. & Schumacher, W. (1998). A Parallel x-y Manipulator with Actuation Redundancy for High-Speed and Active-Stiffness Applications, *Proceeding of the 1998 IEEE International Conference on Robotics & Automation*, pp. 2295-2300, Belgium, May 1998, Leuven.

Kragic, D. & Christensen, H.I. (2005). *Survey on Visual Servoing for Manipulation*. Technical report ISNR KTH/NA/P-02/01-SE, Department of Numerical Analysis and Computing Science, University of Stockolm, Sweden.

Merlet, J.P. (2000). *Parallel Robots,* Klwuer Academic Publishers.

Papanikolopoulos, N. & Khosla, P. (1993). Adaptive Robotic Visual Tracking: Theory and Experiments, *IEEE Transactions on Automatic Control*, Vol. 38, No. 3, March 1993, 429-444.

Santibañez, V. & Kelly, R. (1998). A Class of Nonlinear PID Global Regulators for Robot Manipulators", *Proc. IEEE Int. Conf. on Robotics and Automation*, pp. 3601-3606.

Sebastian, J.M.; Traslosheros, A.; Angel, L.; Roberti, F. & Carelli, R. (2007). *Parallel robot high speed object tracking*. M. Kamel and A. Campilho (Eds.): ICIAR 2007, LNCS 4633, pp. 295.306.

Soria, A.; Garrido, R.; Vásquez, I. & Vázquez ,R. (2006). Architecture for rapid prototyping of visual controllers. *Robotics and Autonomous Systems*, Vol. 54, pp. 486-495.

Spong, M.W.; Hutchinson, S. & Vidyasagar, M. M.W. (2005) *Robot Modeling and Control*, Wiley.

Tsai, L.W. (1999). *Robot Analysis*. John Wiley and Sons Inc.

Weiss, L.; Sanderson, A. & Newman, C. (1987). Dynamic Sensor-Based Control of Robots with Visual Feedback, *IEEE Journal of Robotics and Automation*, Vol. RA-3, No. 5, October 1987, 404-417.

Wen, J. T. & Murphy, S. (1990). *PID control for robot manipulators*, CIRSSE Document # 54, Rensselaer Polytechnic Institute.

Wilson, W.; Williams Hulls, C. & Bell, G. (1996). Relative End-Effector Control Using Cartesian Position Based Visual Servoing, *IEEE Transactions on Robotics and Automation*, Vol. 12, No.5, October 1996, pp. 684-696.

[1] Voss, K.; Ortmann,W. & Suesse, H. (1998). DIAS-Interactive Image Processing System, V 5.0, Friedrich-Schiller-University Jena, Germany.

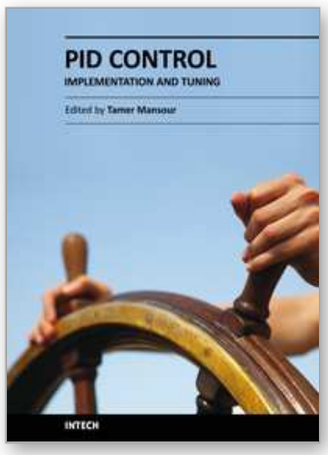

PID Control, Implementation and Tuning

Edited by Dr. Tamer Mansour

ISBN 978-953-307-166-4
Hard cover, 238 pages
Publisher InTech
Published online 19, April, 2011
Published in print edition April, 2011

The PID controller is considered the most widely used controller. It has numerous applications varying from industrial to home appliances. This book is an outcome of contributions and inspirations from many researchers in the field of PID control. The book consists of two parts; the first is related to the implementation of PID control in various applications whilst the second part concentrates on the tuning of PID control to get best performance. We hope that this book can be a valuable aid for new research in the field of PID control in addition to stimulating the research in the area of PID control toward better utilization in our life.

How to reference

In order to correctly reference this scholarly work, feel free to copy and paste the following:

Miguel A. Trujano, Rubén Garrido and Alberto Soria (2011). Stable Visual PID Control of Redundant Planar Parallel Robots, PID Control, Implementation and Tuning, Dr. Tamer Mansour (Ed.), ISBN: 978-953-307-166-4, InTech, Available from: http://www.intechopen.com/books/pid-control-implementation-and-tuning/stable-visual-pid-control-of-redundant-planar-parallel-robots

INTECH
open science | open minds

InTech Europe
University Campus STeP Ri
Slavka Krautzeka 83/A
51000 Rijeka, Croatia
Phone: +385 (51) 770 447
Fax: +385 (51) 686 166
www.intechopen.com

InTech China
Unit 405, Office Block, Hotel Equatorial Shanghai
No.65, Yan An Road (West), Shanghai, 200040, China
中国上海市延安西路65号上海国际贵都大饭店办公楼405单元
Phone: +86-21-62489820
Fax: +86-21-62489821

IntechOpen